

and the persistent spin current that appears with a bias ( $S^C$ ). Fitting variables are the amplitudes  $A$ ,  $B$  and  $C$  ( $C$  is taken as non-zero only for positive biases), and the risetimes  $\tau^A$  and  $\tau^B$ . The other values are fixed and obtained from complementary measurements, such as resonance spectra or time scans from degenerate pump-probe arrangements. We note that the persistent spin current contribution is significant only to spin that has arrived within a time  $T_{\text{ZnSe}}^*$ . Hence, for  $t > T_{\text{ZnSe}}^*$ , the epilayer polarization reflects the precession and the lifetime of the spin current itself, which follows the reservoir spin dynamics. This explains why the average spin polarization in the epilayer is characterized by  $\omega_{\text{GaAs}}$  and  $T_{\text{GaAs}}^*$  although spins reside in ZnSe (and each spin has  $\omega_{\text{ZnSe}}$  and  $T_{\text{ZnSe}}^*$ ).

The changes in net spin transfer with bias are more evident in the absence of spin precession ( $B = 0$ ). In Fig. 3, time scans show an increase in the amplitude of the spin signal in ZnSe as the applied bias is increased, while a reverse bias reduces the number of spins that cross the interface. The most striking influence of the persistent spin flow ( $C$ ) on spin transfer is to introduce an apparent offset to the spin polarization. This offset is due to the long spin lifetimes in GaAs: the reservoir spin population decays only slightly before receiving a boost from the next pump pulse, sourcing a spin current that never reaches zero for  $E > 0$ . The inset in Fig. 3 shows the change in the total spin polarization transferred from the reservoir to the epilayer, where modest electric fields increase spin transfer nearly 500%. About 3/4 of this increase is due to the persistent current; mechanisms A and B, also enhanced by the bias, account for the rest. We also find that the change in spin transfer mimics changes in charge current across the structure (from  $I$ - $V$  measurements), showing that spin and charge motion are coupled in mechanism C.

To see whether similar physics arises from the built-in interfacial electric fields in a p-n junction, we also study spin transfer across a p-GaAs/n-ZnSe heterojunction. As a control, an undoped GaAs substrate is placed together with the p-type substrate in the growth chamber, and 300 nm of n-ZnSe ( $n = 1.5 \times 10^{18} \text{ cm}^{-3}$ ) is deposited simultaneously on both. Figure 4a shows a roughly 4,000% increase in spin transfer due to the heterojunction voltage, compared with the control. Degenerate pump-probe measurements of the ZnSe epilayers are nearly identical, with a slight change in spin lifetime (Fig. 4b). Therefore, the difference in the transferred spin signal amplitudes between the two samples shown in Fig. 4a is not due to differences in the ZnSe epilayers themselves. Unlike the n-doped GaAs 'spin reservoirs', the electron spin lifetimes in the p-doped and undoped GaAs substrates are extremely short<sup>2</sup> (a few picoseconds) so that persistent spin currents do not explain the observed increase. Instead, the data suggest enhancement of spontaneous transfer mechanisms similar to A and B, but with a non-exponential spin

accumulation profile. This is consistent with the observation of electron spin precession at a single frequency corresponding to the g-factor of ZnSe rather than GaAs.

In summary, we show that persistent spin currents appear in biased spin injection studies of GaAs/ZnSe heterostructures. We find that—under electrical bias—the GaAs layer behaves as a coherently rotating spin reservoir that continuously sources current to the ZnSe layer. As a result, the spin transfer efficiency is increased markedly. Furthermore, the magnetic and electric responses become interdependent, thus providing a new paradigm for the future development of magneto-electronic semiconductor devices with qualitatively new functionality. □

Received 28 February; accepted 2 April 2001.

1. Kikkawa, J. M. & Awschalom, D. D. Lateral drag of spin coherence in gallium arsenide. *Nature* **397**, 139–141 (1999).
2. Kikkawa, J. M., Smorchkova, I. P., Samarth, N. & Awschalom, D. D. Room-temperature spin memory in two-dimensional electron gases. *Science* **277**, 1284–1287 (1997).
3. Kikkawa, J. M. & Awschalom, D. D. Resonant spin amplification in n-type GaAs. *Phys. Rev. Lett.* **80**, 4313–4316 (1998).
4. Prinz, G. A. Spin polarized transport. *Phys. Today* **48**, 58–63 (1995).
5. Monzon, F. G. & Roukes, M. L. Spin injection and the local hall effect in InAs quantum wells. *J. Mag. Mater.* **198**, 632–635 (1999).
6. Filip, A. T., Hoving, B. H., Jedema, F. J. & van Wees, B. J. Experimental search for the electrical spin injection in a semiconductor. *Phys. Rev. B* **62**, 9996–9999 (2000).
7. Fiederling, R. *et al.* Injection and detection of a spin-polarized current in a light-emitting diode. *Nature* **402**, 787–790 (1999).
8. Ohno, Y. *et al.* Electrical spin injection in a ferromagnetic semiconductor heterostructure. *Nature* **402**, 790–792 (1999).
9. Malajovich, I., Kikkawa, J. M., Awschalom, D. D., Berry, J. J. & Samarth, N. Coherent transfer of spin through a semiconductor heterointerface. *Phys. Rev. Lett.* **84**, 1015–1018 (2000).
10. Yeganeh, M. S., Qi, J., Yodh, A. G. & Tamargo, M. C. Interface quantum well states observed by three-wave mixing in ZnSe/GaAs heterostructures. *Phys. Rev. Lett.* **68**, 3761–3764 (1992).
11. Schull, K. *et al.* Non-metal in situ and ex situ ohmic contacts to a n-ZnSe. *Semicond. Sci. Technol.* **12**, 485–489 (1997).
12. Malajovich, I., Kikkawa, J. M., Awschalom, D. D., Berry, J. J. & Samarth, N. Resonant amplification of spin transferred across a GaAs/ZnSe interface. *J. Appl. Phys.* **87**, 5073–5075 (2000).

**Acknowledgements**

We thank M. E. Flatte, E. L. Hu, J. M. Kikkawa and H. Kroemer for discussions and suggestions. Work supported by DARPA, ARD, NSF and ONR.

Correspondence and requests for materials should be addressed to D.D.A. (e-mail: awsch@physics.ucsb.edu).

.....  
**Jamming phase diagram for attractive particles**

**V. Trappe\*†, V. Prasad\*, Luca Cipelletti\*†, P. N. Segre\*† & D. A. Weitz\***

\* Department of Physics and DEAS, Harvard University, Cambridge, Massachusetts 02138, USA

.....  
 A wide variety of systems, including granular media, colloidal suspensions and molecular systems, exhibit non-equilibrium transitions from a fluid-like to a solid-like state, characterized solely by the sudden arrest of their dynamics. Crowding or jamming of the constituent particles traps them kinetically, precluding further exploration of the phase space<sup>1</sup>. The disordered fluid-like structure remains essentially unchanged at the transition. The jammed solid can be refluidized by thermalization, through temperature or vibration, or by an applied stress. The generality of the jamming transition led to the proposal<sup>2</sup> of a

† Present addresses: Department of Physics, University of Fribourg, Fribourg, Switzerland (V.T.); Department of Physics, University of Montpellier, Montpellier, France (L.C.); and NASA, Marshall Space Flight Center, Huntsville, Alabama 35812, USA (P.N.S.).

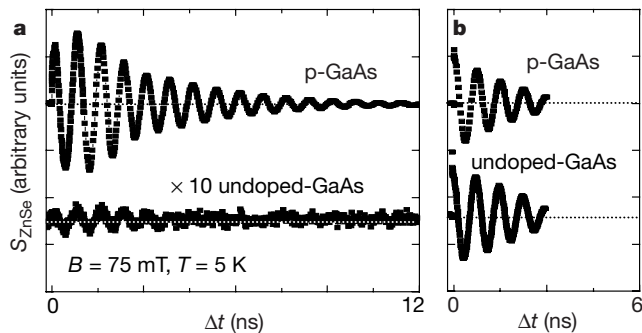


**Figure 4** Time evolution of the spin polarization transfer across a p-GaAs/n-ZnSe heterojunction. Zn p-type doping concentration,  $10^{19} \text{ cm}^{-3}$ . Transfer across an undoped-GaAs/n-ZnSe is shown for comparison. Dotted lines show the zeros, and an offset was added for clarity. **a**, Spins transported across the interface (two-colour pump probe). **b**, Spins excited and measured in the ZnSe epilayer (degenerate pump probe).

unifying description, based on a jamming phase diagram. It was further postulated that attractive interactions might have the same effect in jamming the system as a confining pressure, and thus could be incorporated into the generalized description. Here we study experimentally the fluid-to-solid transition of weakly attractive colloidal particles, which undergo markedly similar gelation behaviour with increasing concentration and decreasing thermalization or stress. Our results support the concept of a jamming phase diagram for attractive colloidal particles, providing a unifying link between the glass transition<sup>3</sup>, gelation<sup>4,5</sup> and aggregation<sup>6–8</sup>.

As an intrinsic parameter to unify the description of all routes to jamming, Liu and Nagel<sup>2</sup> use the density of the system,  $\rho$ . For repulsive systems, a non-uniform, applied stress can increase  $\rho$  and jam athermal systems<sup>1,9</sup>, whereas an osmotic or hydrostatic pressure is required to increase  $\rho$  and jam thermal systems; for attractive systems, the interaction itself increases  $\rho$  and jams the system. Jamming is overcome and the system is fluidized by an increase in temperature or by a uni-directional stress or load that exceeds the yield stress of the material. Therefore, Liu and Nagel<sup>2</sup> propose  $\rho^{-1}$ , temperature,  $T$ , and stress,  $\sigma$ , as the axes of a three-dimensional phase diagram, with the jammed state in the inner octant, as shown in Fig. 1.

Here we consider attractive colloidal particles, and treat the suspending fluid as an inert background; thus the density is set explicitly by the particle volume fraction,  $\phi$ . Temperature still thermalizes the system; however, the degree of thermalization is primarily controlled by the interparticle attractive energy,  $U$ . In this regard, colloidal particles differ markedly from molecular systems that jam; in colloids,  $U$  sets the scale of temperature  $T$ , while the density is set independently by  $\phi$ ; by contrast, in molecular systems,  $U$  and pressure control the density of the system, and  $T$  independently determines the thermalization. Thus, for colloidal particles of radius  $a$ , the axes of the phase diagram become  $\phi^{-1}$ ,  $k_B T/U$  and  $\sigma/\sigma_0$ , where  $\sigma_0 = k_B T/a^3$  sets the scale of the stress in weakly attractive colloid systems. Colloidal suspensions allow us to test the concept of a jamming phase diagram as well its applicability to attractive systems.

To emphasize the generality of the concept, we use data from three vastly different colloid systems—carbon black, polymethyl methacrylate (PMMA), and polystyrene. Each system spans a different range of interparticle interactions, and data from all are amalgamated to complete the phase diagram. The essence of the use of a phase diagram to describe the jamming behaviour is summarized by the optical micrographs of thin samples of carbon black shown in Fig. 2. A highly dispersed, fluid phase of particles is transformed into a jammed solid network by increasing  $\phi$ , increasing  $U$ , or decreasing  $\sigma$ . In each case, the resultant phase transforma-

tion is nearly identical and the structures on the fluid and solid side have very similar appearances. We identify a jammed solid by the existence of a stress-bearing, interconnected network, which results in a low-frequency plateau of the elastic modulus,  $G'_p$  (ref. 10).

As shown in Fig. 2a and b for carbon black, a well-defined transition from fluid-like to solid-like behaviour can be found as either  $\phi$  is increased at constant  $U$ , or  $U$  is increased at constant  $\phi$ . The viscosity,  $\eta$ , diverges as some critical value is approached, whereupon  $G'_p$  increases sharply. The phase boundary at  $\phi_c$  can be identified by the critical-like behaviour of both  $\eta$  and  $G'_p$  for fixed  $U$  (Fig. 2a):

$$\eta = \eta_s(\phi_c - \phi)^{-\nu_\phi} \quad (1)$$

and

$$G'_p = G'_\phi (\phi - \phi_c)^{\nu_\phi} \quad (2)$$

where  $\nu_\phi \approx 0.13$ , and  $\nu_\phi \approx 4.0$  and  $\eta_s$  is the solvent viscosity; both  $G'_\phi$ , and  $\phi_c$  depend on  $U$ . Similarly,  $U_c$  can be identified by the critical-like behaviour of  $\eta$  and  $G'_p$  at fixed  $\phi$ , (Fig. 2b):

$$\eta = \eta_D(U_c - U)^{-\nu_U} \quad (3)$$

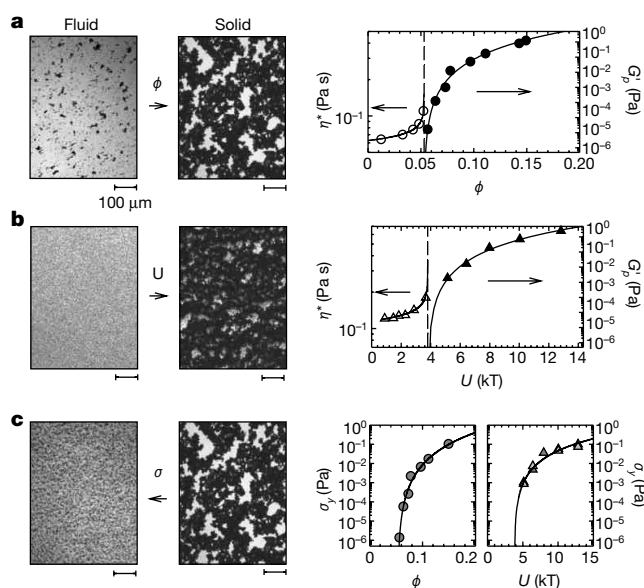


**Figure 2** Control parameters for the jamming transition. Optical micrographs showing the jamming phase transition for carbon black going from the fluid-like to solid-like state.

**a–c**, The volume fraction  $\phi$  increases **(a)**, the interaction energy  $U$  increases **(b)** and the applied stress  $\sigma$  decreases **(c)**. For carbon black there is a divergence of the viscosity and a critical-like onset of the plateau modulus at  $\phi_c = 0.053$  for  $U \approx 10 k_B T$  **(a)** and  $U_c \approx 3.8 k_B T$  for  $\phi = 0.14$  **(b)** whereas the yield stress increases critically with both  $\phi$  and  $U$  **(c)**. The solid lines are results of fits to equations (1), (2), (3), (4), (6) and (7). We note that the points marked as dashed lines in the graphs of **a** and **b** correspond to phase boundaries, while the data themselves are the phase boundaries in the graph of **c**. The exponent for the divergence of the viscosity is rather low; critical-like behaviour, however, is observed over two decades in reduced variables,  $\phi_c - \phi$ , and  $U_c - U$ . The values of  $G'_p$  are obtained from the scaling behaviour of the frequency-dependent moduli, which allow us to determine very weak values of the plateau modulus, which would otherwise require very low-frequency measurements<sup>10</sup>. The yield stresses are calculated using  $G'_p$  and the yield strains,  $\gamma_y$ , which are identified for the onset of strain dependence in  $G'(\omega)$  in oscillatory shear measurements. As the phase boundary is approached,  $\gamma_y$  diverges; this behaviour is typical of a gelling system. The carbon black is suspended in a basestock oil, and the interparticle attraction is controlled through the addition of a dispersant, which adsorbs on the surface of the particles, leading to steric stabilization; increasing concentrations of dispersant lead to decreasing values of  $U$  (ref. 10). These suspensions are very useful for practical studies, serving as excellent benchtop systems to model the behaviour of soot in lubricating oil.

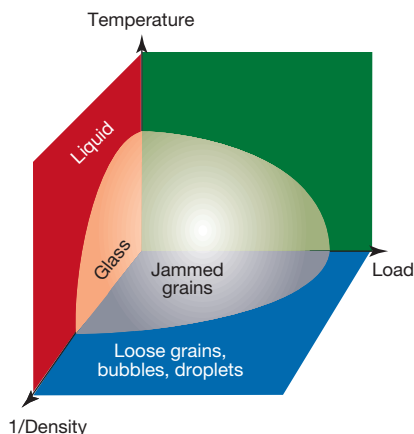


**Figure 1** The jamming phase diagram proposed by Liu and Nagel<sup>2</sup>.

and

$$G'_p = G'_U (U - U_c)^{\nu_U} \tag{4}$$

where again  $\nu_U \approx 0.13$  and  $\nu_U \approx 4.0$ , and  $\eta_D$  is the viscosity of the fully dispersed system; both  $U_c$  and  $G'_U$  depend on  $\phi$ . The power-law behaviour is reminiscent of equilibrium critical phenomena; however, while this similarity is intriguing, jamming is clearly a non-equilibrium transition, and we use these functional forms only as convenient descriptions of the behaviour.

Similar scaling behaviour with a critical-like onset of gelation is observed for the  $\phi$ -dependence of PMMA gels, although the value of the exponent  $\nu_\phi$  depends on the relative range of the depletion interaction  $\xi$ . As the interparticle interaction becomes increasingly attractive, a stress-bearing, interconnected network or gel spanning the system is formed at lower values of  $\phi$ . Dynamic light scattering from these samples shows that the relaxation time due to the motion of clusters of particles diverges as the transition to solid-like behaviour is approached<sup>11</sup>. Thus the solid network is formed by jamming of clusters. The critical values are described by<sup>11</sup>:

$$\phi_c = \phi_0 \exp(-U_c/\alpha k_B T) \tag{5}$$

where  $\alpha$  is a coefficient of order unity, and the values of both  $\alpha$  and  $\phi_0$  depend on  $\xi$ . We use this functional form to define the boundary in the phase diagram, but note that the behaviour can equally well be described by  $\phi \propto U^{-1}$ .

In the limit of  $U/k_B T \ll 1$ , the behaviour approaches that of hard spheres<sup>12</sup>, where monodisperse particles jam to form a solid, stress-bearing network at random close packing,  $\phi_{rcp} = 0.63$ . By contrast, in the limit of  $U/k_B T \gg 1$ , irreversible aggregation results, leading to the formation of fractal clusters<sup>6</sup>. When the fractal clusters fill space, they jam to form an elastic solid. Because the density of a fractal aggregate decreases as the cluster grows, the system will, in principle, form a gel at any volume fraction<sup>7</sup>, so that  $\phi_c$  approaches zero, consistent with equation (5).

The third dimension of the phase diagram is defined by the applied stress,  $\sigma$ , which affects the formation of any solid network

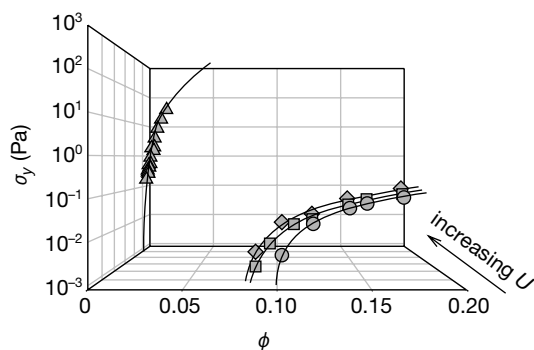


**Figure 3** Cuts along the phase boundary defined by  $\sigma_y$  as a function of  $\phi$  for fixed  $U$  for polymethyl methacrylate (PMMA) and polystyrene gels. For PMMA,  $\xi = 0.28$ ,  $U = 5.0 k_B T$  (circles),  $U = 7.1 k_B T$  (squares),  $U = 8.7 k_B T$  (diamonds); and for polystyrene gels,  $U > 20 k_B T$ . The lines are results of fits to equation (6), with  $\mu_\phi \approx 1.5$  for PMMA and  $\mu_\phi \approx 3.2$  for polystyrene. All yield stresses are identified from the onset of strain dependence in  $G'(\omega)$  in oscillatory shear measurements. The PMMA are stabilized with poly-12-hydroxystearic acid and are suspended in a buoyancy-matched solvent. They are mixed with polystyrene to induce a controlled interparticle attraction owing to the depletion interaction; the strength of the attraction depends on the polymer concentration, whereas its relative range is determined by  $\xi = R_g/a$ , where  $R_g$  is the radius of gyration of the polymer and  $a$  is the particle radius<sup>11,14</sup>. The polystyrene latex is also a buoyancy-matched suspension, to which high concentrations of a divalent salt are added to screen the Coulomb repulsion and induce aggregation; this achieves very high values of  $U$  (refs 7 and 8).

spanning the system, shifting  $\phi_c$  to higher values with increasing  $\sigma$ . For example, for the irreversible aggregation of the polystyrene colloids, a gel will not form at low  $\phi$  if the particles are not buoyancy matched; then  $\phi_c$  becomes significantly greater than zero owing to gravitational stress. In general, a sufficiently large stress will cause a jammed solid sample to yield and flow; thus the yield stress,  $\sigma_y$ , defines the phase boundary. We show both the  $\phi$  and the  $U$  dependencies of  $\sigma_y$  for the carbon black in Fig. 2c. Remarkably, the data are again well described by critical-like functional forms:

$$\sigma_y = \sigma_\phi (\phi - \phi_c)^{\mu_\phi} \tag{6}$$

and

$$\sigma_y = \sigma_U (U - U_c)^{\mu_U} \tag{7}$$

where  $\mu_\phi \approx 3.4$  and  $\mu_U \approx 2.4$ , whereas the values of the coefficients depend on the values of  $U$  (for equation (6)) or  $\phi$  (for equation (7)). These functional forms describe the phase boundaries for the other colloid systems as well, although the values of both the coefficients and exponents depend on the system; we show an example in Fig. 3, where we plot the  $\phi$ -dependence of  $\sigma_y$  for PMMA with different values of  $U$ , and for the polystyrene, for which  $U/k_B T$  becomes very large, so that  $\phi_c = 0$ ; these data reflect cuts along the phase boundary at different values of  $U$ . In all cases, equation (6) describes the functional form, and we use it to define the boundary in the phase diagram.

We plot the full three-dimensional jamming phase diagram for attractive colloidal systems in Fig. 4, where we use the functional forms of equations (5), (6) and (7) to determine the phase boundaries. The values of the coefficients depend on the details of the specific system, and the detailed shape of the phase boundary is likely to be system-dependent. However, the interdependence of  $U_c$ ,  $\phi_c$  and  $\sigma_y$  is robust, allowing us to plot a schematic phase diagram which is a compendium of contributions from different systems and which correctly captures the overall shape and behaviour. The

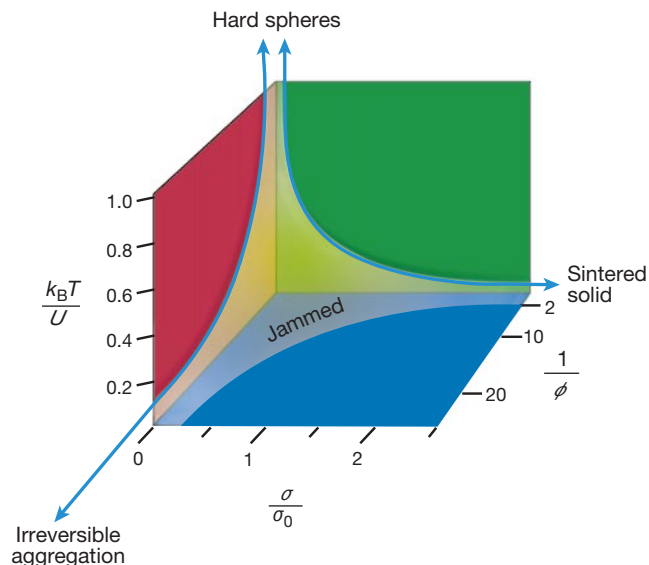


**Figure 4** Composite jamming phase diagram for attractive colloidal particles. We focus on  $k_B T/U < 1$  and  $\phi < 0.5$  and thus do not consider the limits of true hard spheres or of very high concentrations, where more complex behaviour with increasing  $\sigma$  may occur<sup>15</sup>. Data from the three different colloid systems—carbon black, PMMA and polystyrene—are used to construct this phase diagram. It is very difficult to explore the full range of behaviour with any single colloidal system; the phase diagram is therefore a compendium of all systems. We emphasize, however, that the specific phase diagram for any given system may deviate from that shown here, although these deviations will be in the detailed shape, and not the overall behaviour.

existence of this phase diagram supports the fundamental concept of jamming, and confirms the applicability of jamming to describe the behaviour of attractive particles. However, the shape of the experimental phase diagram differs significantly from that originally proposed by Liu and Nagel<sup>2</sup>, having everywhere the opposite curvature, and diverging at each corner. These divergences reflect the particular details of attractive colloidal particles and correspond to irreversible aggregation, where  $\phi_c^{-1}$  is large; to the limit of hard spheres, where  $T/U$  is large; and to high volume fractions of strongly attracting particles that form, for example, sintered solids, where  $\sigma_y$  is large.

The basic concept of a jamming phase transition to describe these diverse phenomena is supported by the similarity in the behaviour as the boundary is crossed; variation in  $\phi$  or  $U$  leads to equivalent critical-like behaviour for the viscosity (equations (1) and (3)) and the plateau modulus (equations (2) and (4)). Similarly, the yield stress defining the phase boundary exhibits critical-like variation in both  $\phi$  and  $U$  (equations (6) and (7)). Moreover, as shown in the micrographs in Fig. 2, the stress plays a similar role to  $\phi$  and  $U$ . This suggests that  $\phi$ ,  $U$  and  $\sigma$  are valid control parameters, and that changes in any of them are equivalent. Additional support for this equivalence comes from the behaviour of the full frequency-dependent storage and loss moduli of solid-like samples,  $G'(\omega)$  and  $G''(\omega)$ , which can be scaled onto identical master curves as either  $\phi$  is varied and  $U$  is held fixed, or as  $U$  is varied and  $\phi$  is held fixed. Similar scaling is observed for the nonlinear stress response as a function of shear rate for the solid-like samples<sup>10</sup>. Finally, both the divergence of the relaxation time of the clusters as gelation approaches, and the shape of the correlation function, are similar to the behaviour observed as the colloidal glass transition is approached, highlighting the equivalence of gelation and the glass transition as examples of the jamming transition<sup>11</sup>.

An integral feature of the jamming transition is the concept of stress-bearing chains<sup>1,9</sup>, which was introduced initially for granular systems, but has since been extended to other systems as well<sup>13</sup>. Attractive colloid systems might provide a useful system with which directly to probe these force chains; unlike more dense repulsive systems, the chains are directly visible as the tenuous colloidal network, with nearly all constituents being part of the stress-bearing structure. By contrast, in repulsive systems, force chains are difficult to observe, because they are obscured by the large number of spectator particles, which are not part of the stress-bearing structure. However, gelling systems show a characteristic divergence of the yield strain,  $\gamma_y$ , as the jamming phase boundary is approached, in contrast to granular systems, which are predicted to be fragile, implying a finite  $\gamma_y$  (ref. 9). The differences in behaviour of the two classes of jammed systems merit further investigation.

Our results confirm that a phase diagram can be used to unify the description of a wide variety of transitions from fluid-like to solid-like behaviour by means of the jamming transition, providing striking confirmation of the proposal of Liu and Nagel<sup>2</sup>. Moreover, our results justify the applicability of the jamming transition in describing systems with attractive interactions, significantly extending the range of materials to which these ideas apply. For practical applications, the jamming phase diagram provides important guidance in the parameters that should be changed to achieve a desired behaviour. We conclude by emphasizing that the concept of jamming is a powerful means to account for a wide range of fluid–solid transitions found in colloid systems and helps rationalize apparently diverse behaviour for very different systems; thus, the colloidal glass transition, colloidal gelation and aggregation can all be put on an equal footing as representations of the jamming transition. □

Received 16 January; accepted 30 April 2001.

1. Edwards, S. F. & Grinev, D. V. in *Jamming and Rheology: Constrained Dynamics on Microscopic and Macroscopic Scales* (eds Liu, A. J. & Nagel, S. R.) 80–93 (Taylor and Francis, New York, 2001).
2. Liu, A. J. & Nagel, S. R. Jamming is not just cool anymore. *Nature* **396**, 21–22 (1998).

3. Pusey, P. N. & van Meegen, W. Observation of a glass transition in suspensions of spherical colloidal particles. *Phys. Rev. Lett.* **59**, 2083–2086 (1987).
4. Grant, M. C. & Russel, W. B. Volume-fraction dependence of elastic moduli and transition temperatures for colloidal silica gels. *Phys. Rev. E* **47**, 2606–2614 (1993).
5. de Rooij, R., van den Ende, D., Duits, M. H. G. & Mellema, J. Elasticity of weakly aggregating polystyrene latex dispersions. *Phys. Rev. E* **49**, 3038–3049 (1994).
6. Weitz, D. A. & Oliveria, M. Fractal structures formed by kinetic aggregation of aqueous gold colloids. *Phys. Rev. Lett.* **52**, 1432–1435 (1984).
7. Carpinetti, M. & Giglio, M. Spinodal-type dynamics in fractal aggregation of colloidal clusters. *Phys. Rev. Lett.* **68**, 3327–3330 (1992).
8. Gisler, T. & Weitz, D. A. Strain hardening of fractal colloidal gels. *Phys. Rev. Lett.* **82**, 1064–1067 (1999).
9. Cates, M. E., Wittmer, J. P., Bouchaud, J. P. & Claudin, P. Jamming, force chains, and fragile matter. *Phys. Rev. Lett.* **81**, 1841–1844 (1998).
10. Trappe, V. & Weitz, D. A. Scaling of the viscoelasticity of weakly attracting particles. *Phys. Rev. Lett.* **85**, 449–452 (2000).
11. Segre, P. N., Prasad, V., Schofield, A. B. & Weitz, D. A. Glass-like kinetic arrest at the colloidal gelation transition. *Phys. Rev. Lett.* (in the press).
12. Pusey, P. N. & van Meegen, W. Phase behaviour of concentrated suspensions of nearly hard colloidal spheres. *Nature* **320**, 340–342 (1986).
13. O'Hern, C. J., Langer, S. A., Liu, A. J. & Nagel, S. R. Force distributions near jamming and glass transitions. *Phys. Rev. Lett.* **86**, 111–114 (2001).
14. Pusey, P. N., Pirie, A. D. & Poon, W. C. K. Dynamics of colloid polymer mixtures. *Physica A* **202**, 322–327 (1993).
15. Melrose, J. R. & Ball, R. C. The pathological behaviour of sheared hard spheres with hydrodynamic interactions. *Europhys. Lett.* **32**, 535–540 (1995).

#### Acknowledgements

We thank S. Nagel and A. Liu for valuable discussions, and for permission to reproduce Fig. 1. This work was supported by Infineum, the NSF and NASA.

Correspondence and requests for materials should be addressed to D.A.W. (e-mail: weitz@deas.harvard.edu).

## Formation of chiral morphologies through selective binding of amino acids to calcite surface steps

C.A. Orme\*, A. Noy\*, A. Wierzbicki†, M. T. McBride\*, M. Grantham‡, H.H. Teng§, P.M. Dove‡ & J.J. DeYoreo\*

\* Chemistry and Material Science Department, Lawrence Livermore National Laboratory, Livermore, California 94551, USA

† Department of Chemistry, University of South Alabama, Mobile, Alabama 36688, USA

‡ Department of Geological Sciences, Virginia Polytechnic Institute and State University, Blacksburg, Virginia 24061, USA

§ Department of Earth and Environmental Sciences, The George Washington University, Washington, District of Columbia 20052, USA

Many living organisms contain biominerals and composites with finely tuned properties, reflecting a remarkable level of control over the nucleation, growth and shape of the constituent crystals<sup>1–6</sup>. Peptides and proteins play an important role in achieving this control<sup>1,7,8</sup>. But the general view that organic molecules affect mineralization through stereochemical recognition, where geometrical and chemical constraints dictate their binding to a mineral, seems difficult to reconcile<sup>4</sup> with a mechanistic understanding, where crystallization is controlled by thermodynamic and kinetic factors<sup>9</sup>. Indeed, traditional crystal growth models emphasize the inhibiting effect of so-called 'modifiers' on surface-step growth, rather than stereochemical matching to newly expressed crystal facets. Here we report *in situ* atomic force microscope observations and molecular modelling studies of calcite growth in the presence of chiral amino acids that reconcile these two seemingly divergent views. We find that enantiomer-specific binding of the amino acids to those surface-step edges that offer the best geometric and chemical fit changes the step-edge